Biospherical Instruments Inc.

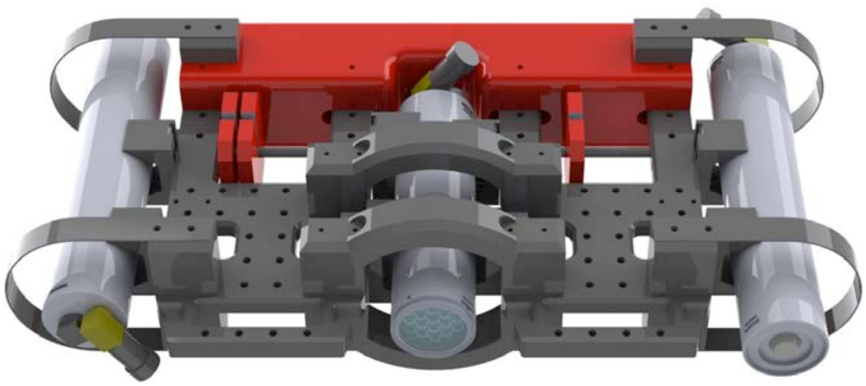

The Compact-Optical Profiling System (C-OPS)

John H. Morrow, Charles R. Booth, Randall N. Lind,

and Stanford B. Hooker

When citing this work, please use the following:

Morrow, J.H., C.R. Booth, R.N. Lind, and S.B. Hooker, 2010: "The Compact Optical Profiling System (C-OPS)." In: J.H. Morrow, S.B. Hooker, C.R. Booth, G. Bernhard, R.N. Lind, and J.W. Brown, Advances in Measuring the Apparent Optical Properties (AOPs) of Optically Complex Waters, *NASA Tech. Memo. 2010–215856,* NASA Goddard Space Flight Center, Greenbelt, Maryland, 42–50.

5340 Riley Street
San Diego, CA 92110-2621 USA

Vox: +1.619.686.1888
Fax: +1.619.686.1887

Net: sales@biospherical.com
Web: www.biospherical.com

Chapter 4

The Compact-Optical Profiling System (C-OPS)

John H. Morrow, Charles R. Booth, and Randall N. Lind
Biospherical Instruments, Inc.
San Diego, California

Stanford B. Hooker
NASA Goddard Space Flight Center
Greenbelt, Maryland

Abstract

The C-OPS instrument successfully integrates a number of new technologies, each focused on different aspects of the practical problem of resolving the optical complexity of the near-shore water column. Although C-OPS represents a significant improvement over BioPRO and other legacy profilers, C-OPS was designed from inception specifically to operate in shallow coastal waters and from a wide variety of deployment platforms. In terms of the mechanics of operating the instrumentation and its behavior during descent, the most significant improvement was to change the basic design for mounting the light sensors from a rocket-shaped deployment system, used in legacy profilers, to the kite-shaped backplane developed for SuBOPS (Chap. 2). This change allowed the flotation to be distributed as a primary hydrobaric buoyancy chamber along the top of the profiler, plus an adjustable secondary set of one or more movable floats immediately below. The primary set provides the upward buoyant thrust to keep the profiler vertically oriented. The secondary set, coupled with an adjustment mechanism perpendicular to the flotation adjustment axis is used to ensure the two light sensors are level. The hydrobaric buoyancy chamber can contain one to three air-filled bladders, which compress slowly and allow the profiler to loiter close to the sea surface, thereby significantly improving the vertical sampling resolution in near-surface waters. Electronically, the system is self-organizing; when initially powered, the aggregator queries each sensor to determine optimal power required for operation over the existing length of the cables and the population of detectors available to the configuration. Typically, each sensor geometry (E_d, E_u, and L_u) is composed of 19 microradiometer detectors, clustered using the MMS hierarchical architecture coordinated through a master aggregator (Chap. 3). Although the use of microradiometers provides improvements in a variety of operational specifications compared to SuBOPS (e.g., reduced electronic noise and slightly faster data acquisition rates), most notable is the reduction in instrument diameter: C-OPS light sensors use a 2.75 in (7 cm) outside diameter housing, which is 27% smaller in diameter than SuBOPS.

4.1 Introduction

The C-OPS instrument is a culmination of several new technologies, each focused on different aspects of resolving the optical complexity of the near-shore water column. Although C-OPS represents a significant improvement over BioPRO and other legacy profilers, it was designed from inception specifically to operate in shallow coastal waters and from a wide variety of platforms ranging from offshore towers, small boats, and ocean-class research vessels. Electronically, the system is self-organizing; when initially powered, the aggregator queries each instrument to determine the optimal power required for operation over the existing length of the cables and the population of detectors available to the configuration.

Typically, each radiometer (E_d, E_u, and L_u) is composed of 19 individual microradiometer detectors, which are controlled as a single cluster using the MMS hierarchical architecture (Chap. 3). The operation of each cluster is coordinated through a master aggregator (Fig. 29), which is usually the (power and telemetry) deck box. Although the use of microradiometers affords improvements in a variety of operational specifications compared to SuBOPS (e.g., reduced electronic noise and slightly faster data acquisition rates), the most notable enhancement is the reduction in size and weight for the optical sensors. The C-OPS sensors have a 2.75 in (7.0 cm) diameter, which is 27% smaller in diameter than the 3.5 in (8.9 cm) PRR-800 sensors used with SuBOPS.

4.2 C-OPS Description

To function well in shallow coastal waters, the C-OPS instrument uses the basic SuBOPS design featuring two parallel sensors mounted symmetrically on either side of a kite-shaped free-fall backplane (Fig. 41). The sensors use microradiometer clusters housed in a 2.75 in (7 cm) in diameter aluminum cylinder that is 27% smaller in diameter than SuBOPS. The pressure transducer for C-OPS is installed on the upper surface of the upwelling radiance or irradiance instruments.

The original twin V-block pairs used to mount the SuBOPS sensors were changed to single elongated blocks for ease in adjusting the pitch orientation of the sensors. As with SuBOPS, roll adjustment is accomplished by controlling the distribution of secondary floats laterally. The lateral floats were redesigned with a slot, so they can slide easily into position and fiberglass nuts are used to hold them in place. A temperature sensor can be mounted on either end cap, but the L_u sensor end cap is preferred, because this permits measurements very close to the sea surface.

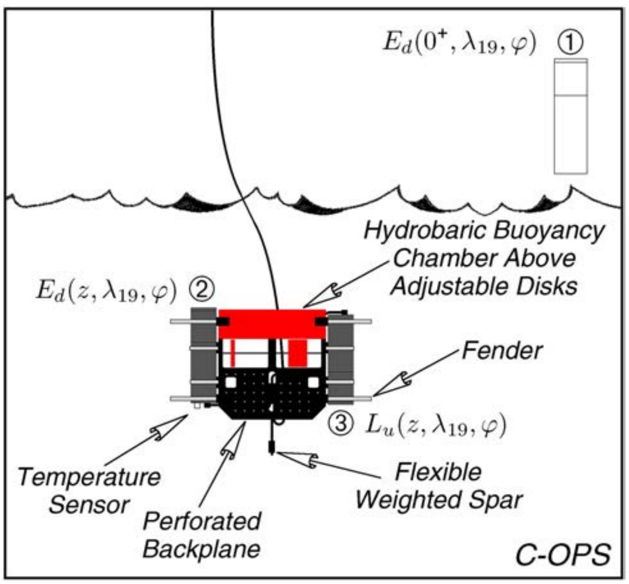

Fig. 41. A schematic of the first C-OPS instrument; newer models have the temperature probe mounted on the L_u endcap to permit measurements as close to the sea surface as possible. Any needed weight is added to a bottom-pointing flexible spar.

The rigid spar used with SuBOPS could be damaged during the recovery of the profiler, so it was replaced by a plastic flexible spar for C-OPS. The flexible spar somewhat protects the L_u aperture in the case of an accidental bottom impact, because it hits the bottom first, but the primary protection for C-OPS is that it is usually tuned for slow descent rates (typically about a $20\,\mathrm{cm\,s^{-1}}$ terminal velocity). The flexibility of the material has additional advantages as a counterpoise in buoyancy control. As with SuBOPS, the main rigid foam buoyancy element features a hollow chamber that can hold 355 mL of air in compressible bladders (Fig. 42) or a combination of bladders and incompressible foam.

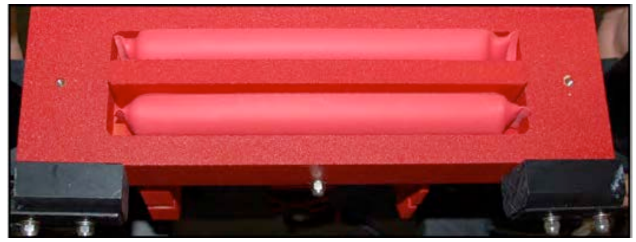

Fig. 42. The C-OPS main buoyancy chamber hollowed out and fitted with two bladders plus a solid foam insert. The removable flotation pieces for adjusting the roll stability of the backplane, with one piece to the left and one to the right, can be seen just below.

4.3 Design

The C-OPS instrument architecture was designed to be inherently flexible. The core elements can be added or removed to accommodate a wide range of research activities. Microradiometers are used as the photodetector elements in all of the light sensors; aggregators ensure that ancillary sensors (e.g., temperature, pressure, pitch, and roll) featured in an instrument are integrated into a single data stream with the microradiometers. As a complete system for the discussion presented here, C-OPS consists of a solar reference with BioSHADE accessory (Chap. 5), two in-water light sensors (selected from E_d, E_u, and L_u), a deck box, and the cabling that connects them all together. Figure 43 shows the interrelationship between the different components used in C-OPS.

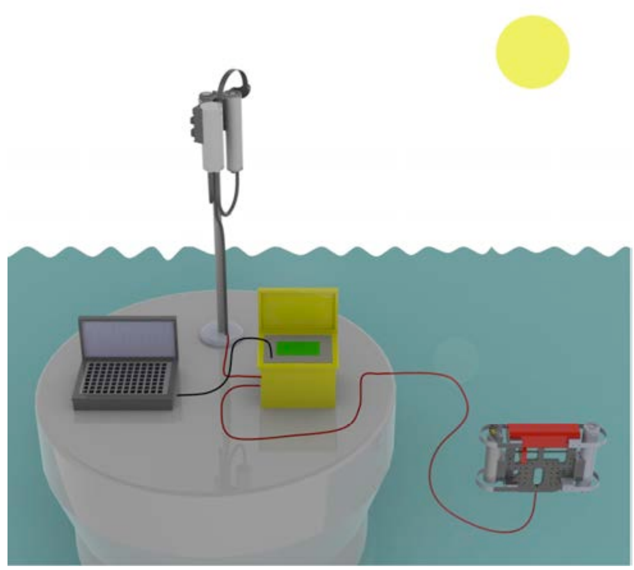

Fig. 43. The C-OPS components configured together showing how the above- and in-water components communicate as sensor groups over corresponding dedicated cables.

Table 3. The specifications for the data-telemetry (sea) cables used with the BioPRO, SuBOPS, and C-OPS free-fall optical instruments. Because SuBOPS was the transition instrument between the legacy (PRR-800) sensors and the new microradiometer sensors, the new cable characteristics were specified using SuBOPS and then evaluated with C-OPS. The three internal synthetics involved are polyethylene (PE), polyurethane (PU), and polypropylene (PP). Conductor specifications are given in American Wire Gauge (AWG) sizes. Bulkhead connectors on the light sensors and deck box are SubConn Micro 6-pin male connectors with female locking sleeves, and SubConn Micro 6-pin female connectors with female locking sleeves, respectively.

Cable Characteristic	*Red Polyester Overbraid Cable*	*Pale Red Polyurethane Cable*
Manufacturer	Cortland Cable Company	Storm Products
Power Conductors	2×20 AWG with PE Insulation	2×20 AWG with PP Insulation
Telemetry Conductors†	4×24 AWG with PE Insulation	4×24 AWG with PP Insulation
Outer Diameter	0.320 in (nominal)	0.320 in (nominal)
Strength Member	Kevlar (1,000 lb breaking rating)	Kevlar (500 lb breaking rating)
Outer Jacket	Black PU with Red Polyester Overbraid	Red Low-Density PU
Connectors	SubConn Micro In-Line (MCIL6)	SubConn Micro In-Line (MCIL6)
Instruments	BioPRO and SuBOPS	SuBOPS and C-OPS

† The four data telemetry conductors are packaged as two individual sets of twisted, shielded pairs.

All C-OPS instruments require a master aggregator (the deck box) to provide power, coordinate data streams from the individual instruments, and deliver data to a computer. There is no requirement to use all components at all times, and because the deck box polls all elements at the time the system is started, it is self organizing; data acquisition does not require a description of the configuration before recording takes place. In the most common C-OPS configuration, a 19-channel solar reference is used to measure spectral global irradiance. A BioSHADE with the optional Biospherical GPS (BioGPS) unit (Chap. 5) can be attached to the reference to add a shadowband capability to the data stream as well as position and time.

Once the system is configured, the RS-485 signals from the above- and in-water components are combined in the deck box and converted to RS-232 communications for computer logging. The RS-232 data are recorded on a laptop computer using commercial software developed by BSI, or custom-built software developed by RSMAS in partnership with NASA. The latter is a continuing testbed for evaluating desired changes in the Protocols associated with deploying the instrumentation.

The deck box provides computer-controlled power to avoid any damage to the instrumentation from improper power-up sequences over varying cable lengths. Shielded six-conductor cables, up to 500 m long for the sea cable and 150 m long for the solar reference surface cable (both fully loaded with 19-channel sensors and all accessories), are used to provide power and return the data from the instruments to the deck box. A standard C-OPS design has a maximum deployment depth of 150 m. The slow descent speed can result in large horizontal displacements of the profiler if subsurface currents are substantial. When coupled with the offset distance needed to avoid platform perturbations, this means cables significantly longer than 150 m are needed to achieve the maximum deployment depth.

Experience with early free-fall designs (e.g., BioPRO and SuBOPS) revealed that the cable was an important component in stability and other behaviors of the instrumentation during descent. The original in-water (sea) cable was designed with an emphasis on strength and ruggedness. Because the profiling systems were deployed by hand, a red polyester outer braid was used to provide a coarse, but easy to handle, surface texture to provide a grip similar to rope (Table 3).

The diameter of instrumentation cable is controlled by the number of conductors required in the application, the presence of a Kevlar strength member, and a waterproofing and protective polyurethane layer. The PRR-800 (BioPRO) electronic design required power and ground, and also included two individual sets of twisted shielded conductors to accommodate the data stream. The shielding is particularly desirable for the solar reference, because it is frequently mounted in the presence of shipboard communications equipment, which are usually active transmitters. The red color made it significantly easier to see the profiler at a distance from the deployment platform during deployments. For use with SuBOPS, the SubConn Microseries of wet-pluggable connectors replaced all connectors originally used for the instrument and deck box.

The red braided cable was robust and easily gripped, which made it easy to use in a wide variety of conditions. Unfortunately, it was also somewhat stiff, and at times, difficult to manage in the time compressed environment of many field campaigns. A recurring problem was the *memory* of the original winding, which made it cumbersome to coil the cable quickly into a bucket. Although the stiffness of the cable provided a somewhat stabilizing influence on free-fall profilers, from a rudder-like effect, the overall influence on instrument pitch was problematic, and the cable was redesigned for the specific purpose of free-fall deployments.

The new sea cable is a paler shade of red. The design retained the original specifications of the conductors in order to remain compatible with legacy instruments, as well as the Kevlar strength member (Table 3). The individual conductor insulation was changed to polypropylene to support high temperature terminations. Additionally, a water blocking compound was incorporated to provide roundness and prevent water propagation in the event of an outer jacket breach. The red braid was removed entirely and a new, low-density, polyurethane, 0.050 in thick outer jacket provides abrasion resistance and waterproofing.

4.4 Operation

The deployment and operation of the C-OPS instrument is situationally dependent on weight distribution and buoyancy, which is itself contingent upon water density. The initial adjustments control platform orientation (pitch and roll). Subsequent adjustments are used primarily to set the proper buoyancy for the system, which determines the magnitude and depth of the terminal velocity, and pitch adjustments to provide bias offsets for currents and the power-telemetry cable. (The pitch axis is perpendicular to the axis connecting the two light sensors and is in the direction of the cabling harness.)

Preparing a C-OPS instrument for use in the field begins with ensuring that the solar reference is properly sited, i.e., the cosine collector has an unobstructed view of the sky, and is cabled to the deck box. The importance of this part of the deployment procedure is presented in Chap. 8. The steps necessary to prepare the C-OPS in-water instrumentation for deployment are as follows: a) connect the power telemetry cable to the Y-cable on the backplane and attach the strain relief to the harness; b) install the desired number of air bladders within the main buoyancy chamber; c) add the desired amount of weight to the counterpoise at the bottom of the instrument; and d) adjust the distribution of the secondary flotation. The instrument is subsequently placed in the water and the descent and vertical tilt observed.

Weight or buoyancy is adjusted as needed to ensure that the instrument is tuned to be almost neutrally buoyant, but biased slightly negative. At this point, the relationship between the near-surface behavior of the instrument and the ultimate terminal velocity is controlled by the ratio of air flotation to weight. The larger this ratio, the longer the system will tend to loiter near the surface. The greater the additional weight, the faster the terminal velocity of the system at depth. These two factors control the wide range of sampling strategies that can be applied to situations such as use in very shallow coastal water or deep oceanographic stations.

When the buoyancy adjustment is complete, the instrument is allowed to drop 1–3 m below the surface (water depth permitting) and the pitch and roll orientations are noted. Secondary flotation is adjusted laterally as needed to zero the roll values. Usually, it is possible to achieve less than $\pm 0.5^\circ$ difference from zero in roll, depending on surface conditions. In calm waters, roll adjustment to within 0.1° is normal. Pitch adjustment uses the geometric relationship between the bottom of the V-block mounts and the backplane. Pivot nuts are loosened and the pitch angle is adjusted on the irradiance side of the instrument to a value that cancels the backplane bias measured during the initial deployment. A plastic dial caliper is used to measure the V-block position relative to the backplane, and then the radiance V-block is adjusted to match. This ensures that the two instruments are parallel relative to the backplane.

The entire attitude adjustment process, from attaching the cable to the initial test profiles, lasts approximately 15–30 min (depending on the experience of the operator and the *in situ* environmental conditions). After the initial tuning, the instrument performance is highly robust and rarely needs adjustment unless the density of the water changes significantly (such as moving from a marine to riverine environment, or moving from the open ocean to the marginal ice zone) or the *in situ* current field changes. Currents pose the most significant challenges, but the main point is to ensure good vertical tilts (less than 5°) close to the sea surface (top 1–5 m). Subsurface currents can degrade data quality, but they usually do not significantly degrade the final data products, so the most important adjustments are those influencing the near-surface behavior of the profiler.

The C-OPS (and SuBOPS) instruments are usually deployed from the stern of a research vessel (although bow deployments are also made to avoid the turbulent mixing that occurs at the stern of a boat). The instrument is first lowered into the water, and allowed to drift away from the ship or to have the ship drift away from the instrumentation. The latter is frequently accomplished by the windage on the vessel. If the profiler does not drift away, short, impulsive headway maneuvers (or *bumps*) of approximately 0.5 kts are used to create enough propeller *wash* to push the profiler or boat away. Ships equipped with thrusters can usually maneuver away from the profiler in a variety of orientations.

The objective of the short impulsive maneuvers is to position the profiler well clear of any possible shadows or reflections caused by the deployment platform. In most cases, three vertical profiles (or *casts*) are acquired, so the profiler needs to be even farther away to allow for some loss of distance when the instrument is pulled back to the surface between casts. In most circumstances, if the profiler is initially placed 30–50 m away from the deployment platform, three casts can be executed without any need for significant repositioning.

A cast is executed by simply releasing the telemetry cable and *paying out* cable at a sufficient rate to prevent it from ever coming under tension. Although the harness of a kite-shaped backplane keeps the instrument in a mostly vertical orientation (so it is not subjected to a significant righting event), the release of the tension associated with the cable still results in oscillations, which can be accentuated or dampened by surface waves. Even brief periods of tension can adversely affect the attitude and descent of the profiler. To ensure this does not occur, the operator leaves some slack cable at the surface. Care is taken to not leave too much free cable in the water, because the cable can move under the ship and become entangled in the propeller or stern thruster intake (if present). To ensure a tangle-free and continuous feed of cable into the water, all of the cable (usually 100–300 m) is coiled in a large bucket or laid out on deck prior to each deployment sequence in such a manner as to minimize entanglements.

Once the profiler reaches the desired depth, which is usually set by the 1% light level or the proximity of the sea bottom, the cable is pulled in to bring the profiler to the surface. Because C-OPS behaves like a kite when the cable is under tension, the profiler has a tendency to ascend vertically (or *pop up*) to the surface without moving significantly closer to the deployment platform (depending on environmental conditions). Small bumps by the ship or a C-HOIST unit (Chap. 8) can be used to haul the cable in faster. If a winch is used, care must be taken to ensure the diameter of the drum is sufficiently large to not damage the cable (C-HOIST does not use a drum).

During a cast, the solar irradiance is monitored for constancy to ensure data collection occurs during stable atmospheric conditions. In addition, the vertical tilt of the profiler is continuously checked to make sure the vertical tilts are to within 5°, particularly near the surface. At depth, the terminal velocity is noted and compared to the desired specification. The amount of negative buoyancy determines the descent speed, as well as the ability of the profiler to sink through high shear features, like the thermocline or a subsurface current.

Once data collection activities are completed, the profiler is washed off with fresh water. The optical apertures are dried with a paper tissue by blotting the surfaces; wiping should be avoided because it can cause scratches. If the cable bucket is large enough, the instrument is wrapped in a white cloth to protect it from solar radiation and placed inside the bucket. Both the bucket and the instrument are then properly secured. If severe weather is expected, the cable and instrument should be brought inside for safe keeping.

4.5 C-OPS Evaluation

The field commissioning of the C-OPS instrument was in predominantly mesotrophic (Case-1) waters. The objectives of the field campaign involved more than just an evaluation of C-OPS, which was done on a not-to-interfere basis with the other cruise priorities. In addition, the station work did not permit simultaneous deployment of equipment, so time differences between when one instrument sampled and when the other sampled was on the order of 24–64 min (with an average of 42 min).

The lack of simultaneity in instrument deployments was not considered a significant detraction to the field commissioning exercise, because a) the measurements were being conducted in Case-1 waters with longer space and time scales for homogeneity, and b) the primary purpose was to test the capabilities of the new profiler under realistic conditions with adequate information to make informed decisions about how to proceed with problems should they arise. Because the continuing refinement of the SuBOPS deployment system was the basis for the C-OPS design, the intercomparison was also an evaluation of how well the engineering concepts associated with kite-shaped deployment systems can be adapted to instruments with differing sizes and weights.

The results of the intercomparison of C-OPS and SuBOPS during the field commissioning campaign is presented in Fig. 44 (for the same eight wavelengths presented in Fig. 15, for which six of the wavelengths are common to Fig. 12). The average UPD for each channel between the two profilers ranges from −5.2% to 6.5%, with an overall average of 1.8% (for the wavelengths plotted in Fig. 44), which is to within the calibration uncertainty. A least-squares linear regression of the data (Fig. 44 inset panel) shows almost one-to-one correspondence with over 95% of the variance explained.

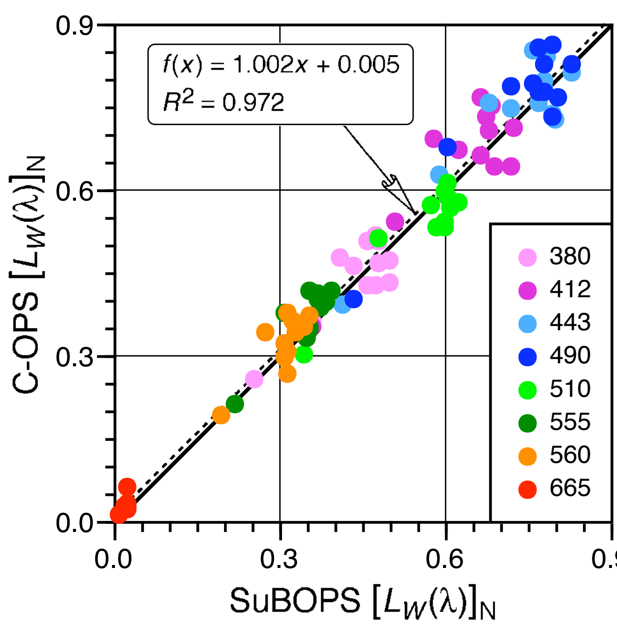

Fig. 44. An intercomparison of the SuBOPS and C-OPS instruments in mostly mesotrophic coastal (Case-1) waters for eight wavelengths, which are given in nanometers. The units for $\left[L_W(\lambda)\right]_{\mathrm{N}}$ are $\mu\mathrm{W\,cm^{-2}\,nm^{-1}\,sr^{-1}}$. The one-to-one line is shown as solid, and the least-squares linear fit to all the data as dashed (regression information is given in the inset panel).

The larger variance in Fig. 44 with respect to the BioPRO and microNESS intercomparison (Fig. 12), which was also in Case-1 waters, is caused by the greater variability of the site and a larger time difference between the measurements by the two profilers. The increase in environmental variability for the C-OPS and SuBOPS intercomparison was caused by an atypical, and rather rapid, evolution in the near-surface waters (upper few meters of the water column). In some cases, the TChl a concentration was changing by more than 5% in a 45 min time period.

The operational evaluation of C-OPS was in predominantly turbid (Case-2 waters with very short time and space scales for homogeneity (Fig. 45). For this activity, the two profilers have almost exactly the same backplane configuration, buoyancy capabilities, and pitch adjustment mechanisms—the primary difference is the use of microradiometers for C-OPS and the PRR-800 technology for SuBOPS. The level of turbidity is well characterized by the average K_d values: 10.7 at 320 nm, decreasing to 0.78 at 560 nm, and then increasing to 3.3 at 780 nm. For this field campaign, simultaneous measurements were permitted during controlled circumstances (e.g., while the ship was anchored and the sea state was relatively calm), so the difficulties associated with spatial inhomogeneity were somewhat offset by an ability to sample the water masses contemporaneously.

Fig. 45. The C-OPS (left) and SuBOPS profilers (right) deployed simultaneously for operational evaluation. The two instrument systems are shown in a river system with a water depth of approximately 6 m.

Although the C-OPS microradiometers have some design features that are a legacy of the technology used in SuBOPS, the microradiometers are essentially new sensors. Consequently, it is appropriate to consider simpler intercomparisons in the operational testing, like the performance of the solar references. This is doubly attractive in this case, because the instruments were deployed simultaneously, so any differences will be much more closely related to true instrument performance issues rather than environmental factors.

An intercomparison of the SuBOPS and C-OPS solar references during the operational evaluation is shown in Fig. 46 for an expanded set of wavelengths than was used in the previous intercomparisons to show more spectral information, but still containing most of the same wavelengths. The average UPD for each channel between the two radiometers ranges from −2.5 to 3.9%, with an overall average of 1.3% (for the wavelengths plotted in Fig. 46), which is to within the calibration uncertainty. A least-squares linear regression of the data (Fig. 46 inset panel) shows almost one-to-one correspondence with over 95% of the variance explained.

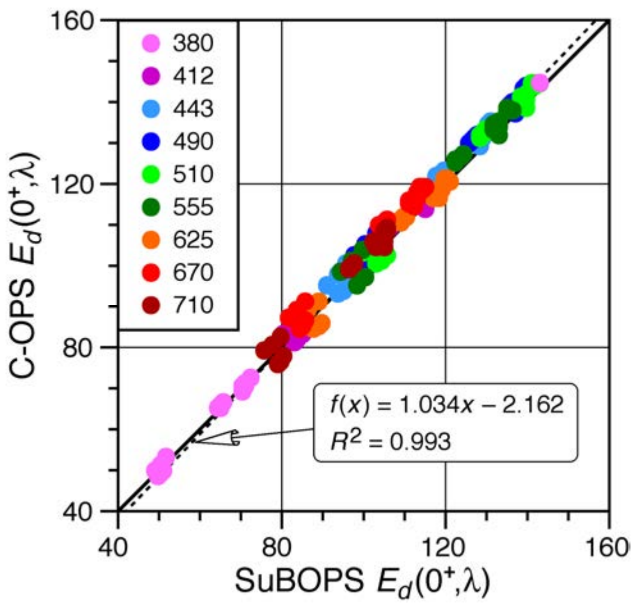

Fig. 46. An intercomparison of the SuBOPS and C-OPS solar references in primarily coastal (Case-2) waters for nine wavelengths given in nanometers. The units for $E_d(0^+)$ are $\mu W\,cm^{-2}\,nm^{-1}$. The one-to-one line is shown in solid, and the least-squares linear fit to all the data in dashed (regression information is given in the inset panel).

The intercomparison of the in-water sensors for the operational evaluation of C-OPS and SuBOPS is presented in Fig. 47 (for the same wavelengths shown in Fig. 46). Ignoring first the far red and NIR plus the far UV, the average UPD for each channel across the 380–625 nm part of the spectrum ranges from −7.0% to 5.6%, with an overall average of −0.8%, which is to within the calibration uncertainty. Considering now all the wavelengths shown in Fig. 47, the average UPD does not change significantly, it is −0.3%, but the range increases in the red and NIR wavelengths and covers −17.4% to 19.7%. A least-squares linear regression of the data (Fig. 47 inset panel) shows almost one-to-one correspondence with almost 95% of the variance explained.

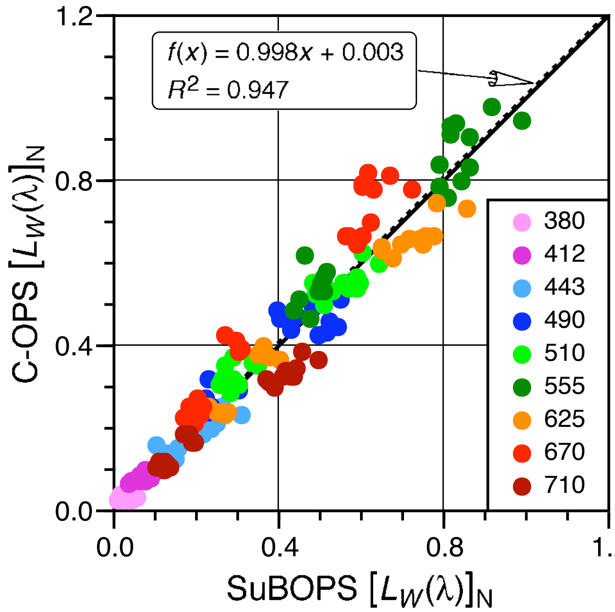

Fig. 47. An intercomparison of the SuBOPS and C-OPS instruments in primarily eutrophic coastal (Case-2) waters for the nine wavelengths in Fig. 46. The units for $\left[L_W(\lambda)\right]_\mathrm{N}$ are $\mu\mathrm{W\,cm^{-2}\,nm^{-1}\,sr^{-1}}$. The one-to-one line is shown as solid, and the least-squares linear fit to all the data as dashed (regression information is given in the inset panel).

If other wavelengths are considered for the intercomparison, the range continues to increase with the addition of the farthest UV and NIR bands, and reaches −50.7% at 780 nm. The reason for this increase is the aforementioned near-surface layer evolution at the sampling site. Although the two profilers were very similar in their capabilities (e.g., they both had vertical tilts to within 1.5°), the C-OPS profiler loiters at the surface better than SuBOPS, so it collected more data in the area that was changing the most. This translated to the C-OPS extrapolation intervals having almost 70% more data (on average) than SuBOPS. For the highly attenuated wavelengths—the far UV, red, and NIR part of the spectrum—this is a very important difference between the two profilers.

4.6 Advancements and Enhancements

While retaining the features of the hydrobaric chamber, the C-OPS backplane was modified to achieve greater terminal velocities by removing a significant amount of the backplane material (which is heavy). The resulting D-shaped frame also eliminates the counterpoise in favor of a horizontal weight-bearing rod that is not within the field of view of upward irradiance instruments. There is sufficient flat surface normal to typical retrieval forces that the instrument will still kite up to the surface for deployments. Using this arrangement, typical terminal velocities exceed $55\,\mathrm{cm\,s^{-1}}$ below 25 m in deep-water profiles.

Although a standard C-OPS profiler can be configured to measure any two-sensor combination of L_u, E_u, and E_d, a specialized backplane providing simultaneous profiling for all three sensor types is being tested. The new design permits the acquisition of all three principal light field components (Fig. 48), so the Q-factor (E_u/L_u) can be measured simultaneously with E_d. The Q-factor is an important parameter for understanding the bidirectional aspects of the underwater light field. Although $Q(\lambda)$ is well understood for Case-1 waters and can be computed using look-up tables based on the solar geometry and the chlorophyll a concentration (Morel and Gentili 1996), no such capability exists for Case-2 (optically complex) waters.

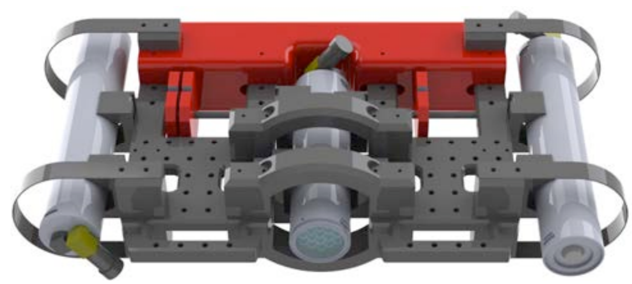

Fig. 48. A schematic of the C-OPS deployment system modified for the simultaneous deployment of three sensors: E_d (left), L_u (center), and E_u (right).

To pursue the goals of simplifying free-fall deployments and removing cable-induced perturbations to profiles, a new sea cable for C-OPS was designed. The objective of the redesign effort was to maximize flexibility and minimize memory via careful selection of jacketing and conductor stranding. Additionally, a half-duplex communication scheme was implemented to allow the removal of one of the twisted pairs used for data telemetry. All internal cable jackets were switched to low-density polyethylene, which is much more flexible than polypropylene; however, this change was made with the tradeoff that heat termination of the cable is no longer supported. The stranding of all conductors was increased to the maximum readily commercially available configurations, which significantly increased the flexibility of the resulting cable. The Kevlar strength member, internal water block, and low-density polyurethane outer jacket were all retained. The outer jacket was thinned slightly to add more flexibility while still providing adequate protection to the internal conductors and a large enough diameter for comfortable handling.

With respect to the entries in Table 3, the following characteristics apply to the new cable:

- *Manufacturer* is Storm Products;
- *Power conductors* are 2×20 AWG with low-density PE insulation;
- *Telemetry conductors* are 2×24 AWG and have low-density PE insulation;
- *Outer diameter* is 0.250 in (nominal);
- *Strength member* is Kevlar (500 lb breaking rating);

Table 4. A comparison of the specifications for the C-OPS (microradiometer) and the BioPRO (PRR-800) profiling systems, with emphasis on the in-water components. The E_s notation denotes a solar reference measuring $E_d(0^+)$. Profiler dimensions do not include the diameter of the sensors. The listed ancillary sensors are in addition to a pressure transducer, which is assumed common to both profiling systems. Profiler dimensions are given as width (W), height (H), and depth (D). The E_s notation denotes an $E_d(0^+)$ sensor.

Specification	*C-OPS*	*BioPRO*
Free-Fall Dynamics	Kite-shaped with hydrobaric buoyancy	Rocket-shaped with buoyant collar
Descent Speed	5–75 $cm\,s^{-1}$	50–100 $cm\,s^{-1}$
Sampling Depth	150 m (300 m optional)	350 m
Trim Adjustment	Individual pitch and roll adjustment	Simultaneous pitch and roll adjustment
Vertical Stability	2.5–5.0° (typical)	3.0–7.0° (typical)
Sampling Resolution	1 cm (less than 1 cm in 0–5 m)	4 cm
Photocurrent-to-Voltage Conversion	Electrometer amplifer with three gain stages: 1, 200, and 40,000	Electrometer amplifer with three gain stages: 1, 300, and 100,000
Analog-to-Digital Conversion	24 bit bipolar sigma-delta running at 4–125 Hz	Shared 16 bit ADC with 1, 16, and 256 gain preamp running at 40 kHz
Dynamic Range	9.5 decades (usable)	9.0 decades (usable)
System Data Rate (one and three sensors)	19 channels at greater than 30 Hz and 57 channels at 15 Hz	19 channels at greater than 20 Hz and 57 channels at 15 Hz
Minimum Detectable Signal	Less than 10^{-15} A (0.5 μV ADC resolution)	Less than 10^{-15} A (1.3 μV ADC resolution while on 256 voltage gain)
Spectral Range	250–1,650 nm†	250–875 nm
Sensor Diameter	7.0 cm	10.2 cm
Sensor Length	34 cm (E_d or E_s) and 25 cm (L_u)	55.9 cm (E_d and L_u) and 37.8 cm (E_s)
Sensor Weight	1.7 kg (E_d or E_s) and 1.6 kg (L_u)	4.8 kg (E_d and L_u) and 3.0 kg (E_s)
Profiler Dimensions	48.7 cm W × 36.0 cm H × 8.9 cm D	30.5 cm W ×55.9 cm H × 14.0 cm D
Profiler Weight	6.8 kg in air (E_d and L_u)	5.9 kg in air (E_d and L_u)
Maximum Depth	150 m (300 m available)	350 m (recommended maximum)
Cosine Collector Error	±3% for $\theta < 60°$; ±5% for $60 \le \theta < 70°$; and ±10% for $70 \le \theta \le 85°$	±2% for $\theta < 60°$; and ±10% for $60 \le \theta < 85°$
Ancillary Profiler Sensors	Water temperature, pitch and roll, internal pressure, and humidity	Water temperature, and pitch and roll

† 1,100–1,650 nm requires InGaAs detectors.

- *Outer jacket* is red low-density PU;
- *Connectors* are SubConn micro in-line (MCIL6 or MCIL4); and
- *Instrument* is C-OPS.

The new cable is connector and conductor compatible with the old cable. What this means is that all old cables will work fine with systems that have been configured to work with the new cable. They can be used as spares, extensions, or primary deployment cables. The new cable will not work with an old system, however. To convert an *old* system to a *new* system, a switch must be flipped in both the deck box and each light sensor. It is not a difficult process, but it is something that should be done at the factory because of O-ring liability and N_2 purges, etc.

4.7 Summary

The C-OPS instrument successfully integrates a number of new technologies, each focused on different aspects of the practical problem of resolving the optical complexity of the near-shore water column. Structured around 19 high-speed microradiometer optical sensors, C-OPS was specifically designed to be compact enough to deploy from small or large vessels by hand.

The profiling system includes separate sensors to measure vertical profiles of spectral downward irradiance, and upwelling radiance or irradiance using a unique, variable-descent, free-fall backplane. A comparison of C-OPS with the legacy BioPRO (PRR-800) profiler is presented in Table 4.

The system is capable of deployments in fresh and marine waters, in depths ranging from 2–150 m. A multichamber, hydrobaric buoyancy system provides very slow initial descent rates with ultimate terminal velocities of 5–75 $\mathrm{cm\,s^{-1}}$, with a typical attitude control to within approximately 2.5° from vertical. Sample speeds of 15 Hz covering more than nine decades of dynamic range ensure that a representative sample is collected even in the shallowest of waters. Unlike earlier versions, the newest counterpoise design uses naval brass weights mounted inboard of the frame, eliminating any potential intrusion into the nadir field-of-view.

Surface loitering, faster terminal velocity at depth, and high data rates result in sufficient sampling to investigate optically diverse, near-surface thin layers, or produce statistically relevant data sets on surface effects. Direct benefits of this new sampling capability include lower uncertainties in the data products across the full dynamic range of the sampling problem set; better accuracy in separating the living and nonliving components of seawater; and an improved understanding of the interaction between the ocean and atmosphere.

The underlying microradiometer technology is notably more compact and more easily expanded than legacy systems (Fig. 49), ensuring a cost-effective expansion path for both AOP profiling instruments and novel systems occupying new roles in the future. The C-OPS technology is an important initial step toward supporting a coupled ocean–atmosphere observing system (i.e., a calibration and validation capability for a combined satellite mission). A mission such as this will likely highlight coastal and open-ocean processes, placing renewed emphasis on making high-quality measurements with equal efficacy in both the near-shore and open-ocean environments.

Fig. 49. Three generations of AOP profilers, which were deployed during one of the Bermuda Atlantic Time Series (BATS) cruises in 2009 (left to right, respectively): Natasha McDonald holding a MicroPro, which was based on the microNESS instrument; Stanford Hooker holding the first C-OPS unit; and Vincenzo Vellucci holding an SPMR. A second SPMR is on deck in the foreground at left.

Acknowledgments

The success of the data acquisition and data processing capabilities presented here would not have been possible without funding support from the NASA OBB Program Office. The microradiometer, aggregator, and associated systems were developed by Biospherical Instruments, Inc., with funding from the NASA SBIR Program under contract NNG06CA03C entitled "*In Situ* Radiometers: Smaller, Faster, and Scalable to Hyperspectral." The preparation of the manuscript and its final level of completeness benefitted significantly from the technical editing expertise of Elaine Firestone whose attentiveness to detail, and good cheer, are greatly appreciated.

Glossary

3GμR Three-Gain Microradiometer

A/D Analog-to-Digital
ADC Analog-to-Digital Converter
AERONET Aerosol Robotic Network
AOI Angle of Incidence
AOPs Apparent Optical Properties
ASCII American Standard Code for Information Interchange
AWG American Wire Gauge

BATS Bermuda Atlantic Time Series
BioGPS Biospherical Global Positioning System
BioOPS Biospherical Optical Profiling System
BioPRO Biospherical Profiler
BioSHADE Biospherical Shadowband Accessory for Diffuse Irradiance
BioSOPE Biogeochemistry and Optics South Pacific Experiment
BioSORS Biospherical Surface Ocean Reflectance System
BOUSSOLE *Bouée pour l'acquisition de Séries Optiques à Long Terme* (literally translated from French as the "buoy for the acquisition of a long-term optical series.")

CCGS Canadian Coast Guard Ship
CCW Counterclockwise
CDR Climate-quality Data Record
CERBERUS Compact Environmental Radiometer Buoyancy Enhancements for Rate-Adjusted Underwater Sampling
C-HOIST Cable Hauler for Optical *In Situ* Technologies
C-OPS Compact-Optical Profiling System
COTS Commercial Off-The-Shelf
CSTARS Center For Southeastern Tropical Advanced Remote Sensing
CVO Calibration and Validation Office
CW Clockwise

DARR-94 The first SeaWiFS Data Analysis Round Robin
DARR-00 The second SeaWiFS Data Analysis Round Robin

EOS Earth Observing System
EPIC Enhanced Performance Instrument Class

FAFOV Full-Angle Field of View
FEL Not an acronym, but a lamp designator.
FPA Filter-Photodetector Assemblies
FOV Field of View
FWHM Full Width at Half Maximum

GPS Global Positioning System
GSFC Goddard Space Flight Center

HD Housing Diameter

ICESCAPE Impacts of Climate on Ecosystems and Chemistry of the Arctic Pacific Environment
IOPs Inherent Optical Properties
IR Infrared

LCD Liquid Crystal Display
LED Light Emitting Diode
LoCNESS Low-Cost NASA Environmental Sampling System
LOV *Laboratoire d'Océanographie de Villefranche*

MERIS Medium Resolution Imaging Spectrometer
microSAS micro-Surface Acquisition System
microSD Microsecure Digital (card)
microNESS micro-NASA Environmental Sampling System
miniNESS miniature NASA Environmental Sampling System
MMS Multiple Microradiometer System
MOBY Marine Optical Buoy
MODIS Moderate Resolution Imaging Spectroradiometer
MODIS-A Moderate Resolution Imaging Spectroradiometer-Aqua
MODIS-T Moderate Resolution Imaging Spectroradiometer-Terra

NASA National Aeronautics and Space Administration
NEI Noise Equivalent Irradiance
NER Noise Equivalent Radiance
NIR Near Infrared
NIST National Institute of Standards and Technology
NMEA National Marine Electronics Association
NPT National Pipe Tapered

OBB Ocean Biology and Biogeochemistry
OCTS Ocean Color and Temperature Scanner
OSPREy Optical Sensors for Planetary Radiant Energy
OXR OSPREy Transfer Radiometer

PAR Photosynthetically Available Radiation
PCA Printed Circuit Assembly
PE Polyethylene
PGA Programmable Gate Array
POLDER Polarization and Directionality of the Earth's Reflectance
PP Polypropylene
PRR Profiling Reflectance Radiometer
psia Pressure per Square Inch Absolute
PU Polyurethane
PURLS Portable Universal Radiometer Light Source

QA Quality Assurance

RPD Relative Percent Difference
RSMAS Rosenstiel School of Marine and Atmospheric Science
RTD Resistance Temperature Detector
R/V Research Vessel

SAS Surface Acquisition System
SBIR Small Business Innovation Research
SeaBASS SeaWiFS Bio-optical Archive and Storage System
SeaFALLS SeaWiFS Free-Falling Advanced Light Level Sensors
SeaPRISM SeaWiFS Photometer Revision for Incident-Surface Measurements
SeaSAS SeaWiFS Surface Acquisition System
SeaWiFS Sea-viewing Wide Field-of-view Sensor
SHALLO Scalable Hydro-optical Applications for Light-Limited Oceanography
SIRREX SeaWiFS Intercalibration Round-Robin Experiment
SPI Serial Peripheral Interface
SPMR SeaWiFS Profiling Multichannel Radiometer
SQM SeaWiFS Quality Monitor
SS Stainless Steel
STAR Standardized Technologies for Applied Radiometry
SuBOPS Submersible Biospherical Optical Profiling System
SUnSAS SeaWiFS Underway Surface Acquisition System
SWIR Short-Wave Infrared
SZA Solar Zenith Angle

T-MAST Telescoping Mount for Advanced Solar Technologies

UAV Unmanned Aerial Vehicle
UPD Unbiased Percent Difference
USB Universal Serial Bus
USCGC United States Coast Guard Cutter
UTC Universal Time Coordinated
UV Ultraviolet

XTRA Expandable Technologies for Radiometric Applications

Symbols

C_a Chlorophyll a concentration.
$c_b(\lambda)$ The angular response error of the solar reference.
$C_c(\lambda)$ The spectral calibration coefficient.
$c_d(\lambda)$ The angular response error of the solar reference when measuring global irradiance.
$c_i(\lambda)$ The angular response error of the solar reference when exposed to isotropic radiation.

d The distance between the lamp and the diffuser faceplate.
$\bar{D}(\lambda)$ The average bias or dark voltage.

$E(\lambda)$ Spectral irradiance.
$E(z,\lambda)$ Spectral irradiance at a depth z.
$E(0^+,\lambda)$ The in-air spectral irradiance just above the sea surface.
$E(0^-,\lambda)$ The in-water spectral irradiance at null depth ($z = 0^-$).
$E_0(\lambda)$ The direct-normal spectral irradiance outside the Earth's atmosphere (irradiance on a plane perpendicular to the detector–Sun direction).
$E_a(0^+,\lambda)$ The spectral irradiance at the solar reference when the centers of the solar disk, shadowband, and diffuser are aligned and direct sunlight is completely occluded (at time t_v).
$E_b(0^+,\lambda)$ The direct-horizontal spectral irradiance (irradiance on a horizontal plane from direct solar illumination).
$E_{\mathrm{cal}}(\lambda,t_i)$ The spectral calibrated irradiance.
$E_d(z,\lambda)$ The in-water spectral downward irradiance profile.
$E_d(0^+,\lambda)$ The spectral global solar irradiance (from the Sun and sky on a horizontal plane).
$E_d^B(0^+,\lambda)$ The global solar irradiance measured by a bow sensor.
$E_d^S(0^+,\lambda)$ The global solar irradiance measured by a stern sensor.
$E_i(0^+\lambda)$ The spectral diffuse (sky) irradiance (irradiance from the sky on a horizontal plane).
$E_k(0^+,\lambda)$ The hypothetical spectral irradiance at the solar reference for the segment of the sky that is shaded by the shadowband when the band is at time t_v and the shadowband is at angle v.
$E_n(0^+,\lambda)$ The direct-normal spectral irradiance (irradiance on a plane perpendicular to the detector–Sun direction).
$E_p(0^+,\lambda)$ The spectral irradiance at the solar reference at time t_v when the band is at shadowband angle v and not blocking direct sunlight.
$E'_{p_B}(0^+,\lambda)$ An extrapolated spectral irradiance (at the solar reference) at time t_M using an interval denoted B.
$E'_{p_E}(0^+,\lambda)$ An extrapolated spectral irradiance (at the solar reference) at time t_M using an interval denoted E.
E_s A solar reference sensor.

$I_f(\lambda)$ The spectral immersion factor.

$K(\lambda)$ The spectral diffuse attenuation coefficient.
$K_d(\lambda)$ The spectral diffuse attenuation coefficient computed from $E_d(z,\lambda)$.

$L_i(0^+,\lambda)$ The spectral indirect (or sky) radiance reaching the sea surface.
$L_p(0^+,\lambda)$ The radiance of the plaque.
$L_T(0^+,\lambda)$ The (total) radiance above the sea surface.
$L_u(\lambda)$ The upwelled spectral radiance.
$L_u(z,\lambda)$ The upwelled spectral radiance at depth z.
$L_W(\lambda)$ The spectral radiance leaving the sea surface from below (the water-leaving radiance).
$\hat{L}_W(\lambda)$ The spectral water-leaving radiance derived from an above-water sampling method.
$\tilde{L}_W(\lambda)$ The spectral water-leaving radiance derived from an in-water sampling method.
$[L_W(\lambda)]_{\mathrm{N}}$ The spectral normalized water-leaving radiance.

M The point (in time) when the centers of the Sun, shadowband, and collector are all aligned.
$m(\theta)$ The relative optical airmass.

N_P The number of photodetectors.
$n_w(\lambda)$ The spectral refractive index of water, which is also a function of S and T.

$\mathfrak{P}$ The in-water radiometric quantities in physical units (L_u, E_d, or E_u).
P_e The packing efficiency of microradiometers into a cylinder.
$\mathfrak{P}(z,\lambda,t_0)$ A radiometric parameter (L_u, E_d, or E_u) as it would have been recorded at all depths z at the same time t_0.
$\mathfrak{P}(0^-,\lambda)$ A subsurface radiometric quantity (L_u, E_d, or E_u) at null depth $z = 0^-$.

Q_n Nadir-viewing measurements.

R_d Radius of the diffuser.
$R_{\rm rs}$ Remote sensing reflectance.
$\Re$ The effects of reflection and refraction.
$\Re_0$ The $\Re$ term evaluated at nadir, i.e., $\theta' = 0$
S Salinity.
t Time.
T Water temperature.
t_0 A reference time (generally chosen to coincide with the start of a measurement sequence).
t_i A specific time.
$T_s(\lambda)$ The spectral transmittance of the water surface to downward irradiance.
t_υ The time when the shadowband is at angle υ.
$V(\lambda, t_i)$ Spectral digitized voltages (in counts).
W Wind speed.
x The horizontal axis (abscissa).
X An arbitrary reference measurement.
Y An arbitrary measurement to be investigated.
z The vertical (depth) coordinate, where the depth is the height of water above the cosine collectors.
z_c The critical depth.
θ Solar zenith angle.
θ' The above-water viewing angle (ϑ) refracted by the air–sea interface.
ϑ The radiometer pointing angle with respect to the vertical axis, z.
ϑ' The angle ϑ measured with respect to the zenith.
λ Wavelength.
ρ The surface reflectance factor.
$\tau(\lambda)$ The spectral optical depths of all scatters and absorbers in the atmosphere.
$\tau_A(\lambda)$ The aerosol optical depth.
$\tau_R(\lambda)$ The Rayleigh optical depth.
$\tau_X(\lambda)$ Other scatters and absorbers at optical depth.
ϕ The solar azimuth angle.
φ The perturbations (or tilts) in vertical alignment, which can change the pointing angles.
ϕ' An angle away from the Sun (here either 90° or 135°).
ϕ^- An angle 90° counterclockwise away from the Sun.
ϕ^+ An angle 90° clockwise away from the Sun.
ψ The RPD value.

References

Antoine, D., F. d'Ortenzio, S.B. Hooker, G. Bécu, B. Gentili, D. Tailliez, and A.J. Scott, 2008: Assessment of uncertainty in the ocean reflectance determined by three satellite ocean color sensors (MERIS, SeaWiFS and MODIS-A) at an offshore site in the Mediterranean Sea (BOUSSOLE project). *J. Geophys. Res.,* **113,** C07013, doi:10.1029/2007JC004472, 2008.

Austin, R.W., 1974: "The Remote Sensing of Spectral Radiance from Below the Ocean Surface." In: *Optical Aspects of Oceanography,* N.G. Jerlov and E.S. Nielsen, Eds., Academic Press, London, 317–344.

Bailey, S.W., S.B. Hooker, D. Antoine, B.A. Franz, P.J. Werdell, 2008: Sources and assumptions for the vicarious calibration of ocean color satellite observations. *Appl. Opt.,* **47,** 2,035–2,045.

Booth, C.R., T. Mestechkina, and J.H. Morrow, 1994: Errors in the reporting of solar spectral irradiance using moderate bandwidth radiometers: an experimental investigation. *SPIE Ocean Optics XII,* **2258,** 654–662.

Carder, K.L., and R.G. Steward, 1985: A remote sensing reflectance model of a red tide dinoflagellate off West Florida. *Limnol. Oceanogr.,* **30,** 286–298.

Clark, D., H.R. Gordon, K.J. Voss, Y. Ge, W. Broenkow, and C. Trees, 1997: Validation of atmospheric correction over the oceans. *J. Geophys. Res.,* **102,** 17,209–17,217.

Claustre, H., A. Sciandra, and D. Vaulot, 2008: Introduction to the special section bio-optical and biogeochemical conditions in the South East Pacific in late 2004: The BIOSOPE program. *Biogeosci.,* **5,** 679–691.

Doyle, P.J., S.B. Hooker, G. Zibordi, and D. van der Linde, 2003: Validation of an In-Water, Tower-Shading Correction Scheme. *NASA Tech. Memo. 2003–206892, Vol. 25,* S.B. Hooker and E.R. Firestone, Eds., NASA Goddard Space Flight Center, Greenbelt, Maryland, 32 pp.

Fougnie, B., R. Frouin, P. Lecomte, and P-Y. Deschamp, 1999: Reduction of skylight reflection effects in the above-water measurement of diffuse marine reflectance. *Appl. Opt.,* **38,** 3,844–3,856.

Gordon, H.R., and D.K. Clark, 1981: Clear water radiances for atmospheric correction of coastal zone color scanner imagery. *Appl. Opt.,* **20,** 4,175–4,180.

——, and K. Ding, 1992: Self-shading of in-water optical instruments. *Limnol. Oceanogr.,* **37,** 491–500.

Holben, B.N., T.F. Eck, I. Slutsker, D. Tanré, J.P. Buis, A. Setzer, E. Vermote, J.A. Reagan, Y.J. Kaufman, T. Nakajima, F. Lavenu, I. Jankowiak, and A. Smirnov, 1998: AERONET—A federated instrument network and data archive for aerosol characterization. *Remote Sens. Environ.,* **66,** 1–16.

Hooker, S.B., 2000: "Stability Monitoring of Field Radiometers Using Portable Sources." In: G.S. Fargion and J.L. Mueller, Ocean Optics Protocols for Satellite Ocean Color Sensor Validation, Revision 2. *NASA Tech. Memo. 2000–209966,* NASA Goddard Space Flight Center, Greenbelt, Maryland, 57–64.

——, 2002: "Stability Monitoring of Field Radiometers Using Portable Sources." In: Mueller, J.L., and 39 Co-authors, Ocean Optics Protocols for Satellite Ocean Color Sensor Validation, Revision 3, Volume 1, J.L. Mueller and G.S. Fargion, Eds., *NASA Tech. Memo. 2002–210004/Rev3/Vol1,* NASA Goddard Space Flight Center, Greenbelt, Maryland, 91–99.

——, and W.E. Esaias, 1993: An overview of the SeaWiFS project. *Eos, Trans., Amer. Geophys. Union,* **74,** 241–246.

——, and J. Aiken, 1998: Calibration evaluation and radiometric testing of field radiometers with the SeaWiFS Quality Monitor (SQM). *J. Atmos. Oceanic Tech.,* **15,** 995–1,007.

——, G. Zibordi, G. Lazin, and S. McLean, 1999: The SeaBOARR-98 Field Campaign. *NASA Tech. Memo. 1999–206892, Vol. 3,* S.B. Hooker and E.R. Firestone, Eds., NASA Goddard Space Flight Center, Greenbelt, Maryland, 40 pp.

——, and G. Lazin, 2000: The SeaBOARR-99 Field Campaign. *NASA Tech. Memo. 2000–206892, Vol. 8,* S.B. Hooker and E.R. Firestone, Eds., NASA Goddard Space Flight Center, 46 pp.

——, and S. Maritorena, 2000: An evaluation of oceanographic radiometers and deployment methodologies. *J. Atmos. Oceanic Technol.,* **17,** 811–830.

——, and C.R. McClain, 2000: The calibration and validation of SeaWiFS data. *Prog. Oceanogr.,* **45,** 427–465.

——, and A. Morel, 2003: Platform and environmental effects on above- and in-water determinations of water-leaving radiances. *J. Atmos. Ocean. Technol.,* **20,** 187–205.

——, and G. Zibordi, 2005: Platform perturbations in above-water radiometry. *Appl. Opt.,* **44,** 553–567.

——, H. Claustre, J. Ras, L. Van Heukelem, J-F. Berthon, C. Targa, D. van der Linde, R. Barlow, and H. Sessions, 2000a: The First SeaWiFS HPLC Analysis Round-Robin Experiment (SeaHARRE-1). *NASA Tech. Memo. 2000–206892, Vol. 14,* S.B. Hooker and E.R. Firestone, Eds., NASA Goddard Space Flight Center, Greenbelt, Maryland, 42 pp.

——, G. Zibordi, J-F. Berthon, S.W. Bailey, and C.M. Pietras, 2000b: The SeaWiFS Photometer Revision for Incident Surface Measurement (SeaPRISM) Field Commissioning. *NASA Tech. Memo. 2000–206892, Vol. 13,* S.B. Hooker and E.R. Firestone, Eds., NASA Goddard Space Flight Center, Greenbelt, Maryland, 24 pp.

——, ——, ——, D. D'Alimonte, S. Maritorena, S. McLean, and J. Sildam, 2001: Results of the Second SeaWiFS Data Analysis Round Robin, March 2000 (DARR-00). *NASA Tech. Memo. 2001–206892, Vol. 15,* S.B. Hooker and E.R. Firestone, Eds., NASA Goddard Space Flight Center, Greenbelt, Maryland, 71 pp.

——, S. McLean, J. Sherman, M. Small, G. Lazin, G. Zibordi, and J.W. Brown, 2002a: The Seventh SeaWiFS Intercalibration Round-Robin Experiment (SIRREX-7), March 1999. *NASA Tech. Memo. 2002–206892, Vol. 17,* S.B. Hooker and E.R. Firestone, Eds., NASA Goddard Space Flight Center, Greenbelt, Maryland, 69 pp.

——, G. Lazin, G. Zibordi, and S. McLean. 2002b. An evaluation of above- and in-water methods for determining water-leaving radiances. *J. Atmos. Oceanic Technol.,* **19,** 486–515.

——, G. Zibordi, J-F. Berthon, D. D'Alimonte, D. van der Linde, and J.W. Brown, 2003: Tower-Perturbation Measurements in Above-Water Radiometry. *NASA Tech. Memo. 2003–206892, Vol. 23,* S.B. Hooker and E.R. Firestone, Eds., NASA Goddard Space Flight Center, Greenbelt, Maryland, 35 pp.

——, ——, ——, and J.W. Brown, 2004: Above-water radiometry in shallow, coastal waters. *Appl. Opt.,* **43,** 4,254–4,268.

——, L. Van Heukelem, C.S. Thomas, H. Claustre, J. Ras, L. Schlüter, J. Perl, C. Trees, V. Stuart, E. Head, R. Barlow, H. Sessions, L. Clementson, J. Fishwick, C. Llewellyn, and J. Aiken, 2005: The Second SeaWiFS HPLC Analysis Round-Robin Experiment (SeaHARRE-2). *NASA Tech. Memo. 2005–212785,* NASA Goddard Space Flight Center, Greenbelt, Maryland, 112 pp.

——, ——, ——, ——, ——, ——, L. Clementson, D. Van der Linde, E. Eker-Develi, J-F. Berthon, R. Barlow, H. Sessions, J. Perl, and C. Trees, 2009: The Third SeaWiFS HPLC Analysis Round-Robin Experiment (SeaHARRE-3). *NASA Tech. Memo. 2009,* NASA Goddard Space Flight Center, Greenbelt, Maryland, 97 pp.

——, G. Bernhard, J.H. Morrow, C.R. Booth, T. Cromer, R.N. Lind, and V. Quang, 2010: Optical Sensors for Planetary Radiant Energy (OSPREy): Calibration and Validation of Current and Next-Generation NASA Missions. *NASA Tech. Memo.,* NASA Goddard Space Flight Center, Greenbelt, Maryland, (in prep.).

Johnson, B.C., S.S. Bruce, E.A. Early, J.M. Houston, T.R. O'Brian, A. Thompson, S.B. Hooker, and J.L. Mueller, 1996: The Fourth SeaWiFS Intercalibration Round-Robin Experiment (SIRREX-4), May 1995. *NASA Tech. Memo. 104566, Vol. 37,* S.B. Hooker and E.R. Firestone, Eds., NASA Goddard Space Flight Center, Greenbelt, Maryland, 65 pp.

——, F. Sakuma, J.J. Butler, S.F. Biggar, J.W. Cooper, J. Ishida, and K. Suzuki, 1997: Radiometric Measurement Comparison Using the Ocean Color Temperature Scanner (OCTS) Visible and Near Infrared Integrating Sphere. *J. Res. NIST,* **102,** 627–646.

——, P-S. Shaw, S.B. Hooker, and D. Lynch, 1998: Radiometric and engineering performance of the SeaWiFS Quality Monitor (SQM): A portable light source for field radiometers. *J. Atmos. Oceanic Tech.,* **15,** 1,008–1,022.

——, H.W. Yoon, S.S. Bruce, P-S. Shaw, A. Thompson, S.B. Hooker, R.E. Eplee, Jr., R.A. Barnes, S. Maritorena, and J.L. Mueller, 1999: The Fifth SeaWiFS Intercalibration Round-Robin Experiment (SIRREX-5), July 1996. *NASA Tech. Memo. 1999–206892, Vol. 7,* S.B. Hooker and E.R. Firestone, Eds., NASA Goddard Space Flight Center, 75 pp.

McClain, C.R., W.E. Esaias, W. Barnes, B. Guenther, D. Endres, S.B. Hooker, G. Mitchell, and R. Barnes, 1992: Calibration and Validation Plan for SeaWiFS. *NASA Tech. Memo. 104566, Vol. 3,* S.B. Hooker and E.R. Firestone, Eds., NASA Goddard Space Flight Center, Greenbelt, Maryland, 41 pp.

——, G.C. Feldman, and S.B. Hooker, 2004: An overview of the SeaWiFS project and strategies for producing a climate research quality global ocean bio-optical time series. *Deep Sea Res. II,* **51,** 5–42.

Mobley, C.D., 1999: Estimation of the remote-sensing reflectance from above-surface measurements. *Appl. Opt.,* **38,** 7,442–7,455.

Morel, A., and L. Prieur, 1977: Analysis of variations in ocean color. *Limnol. Oceanogr.,* **22,** 709–722.

——, and B. Gentili, 1996: Diffuse reflectance of oceanic waters, III. Implication of bidirectionality for the remote sensing problem. *Appl. Opt.,* **35,** 4,850–4,862.

——, and J.L. Mueller, 2002: "Normalized Water-Leaving Radiance and Remote Sensing Reflectance: Bidirectional Reflectance and Other Factors." In: J.L. Mueller and G.S. Fargion, Ocean Optics Protocols for Satellite Ocean Color Sensor Validation, Revision 3, Volume 2. *NASA Tech. Memo. 2002–210004/Rev3–Vol2,* NASA Goddard Space Flight Center, Greenbelt, Maryland, 183–210.

Morrow, J.H., M.S. Duhig, C.R. Booth, 1994: Design and evaluation of a cosine collector for a SeaWiFS-compatible marine reflectance radiometer. *SPIE Ocean Optics XII,* **2258,** 879–886.

——, M. Duhig, and C.R. Booth, 1994: Design and Evaluation of a cosine collector for a SeaWiFS-compatible Marine Reflectance Radiometer. *SPIE Ocean Optics XII,* **2258,** 879–886.

Mueller, J.L., 1993: The First SeaWiFS Intercalibration Round-Robin Experiment, SIRREX-1, July 1992. *NASA Tech. Memo. 104566, Vol. 14,* S.B. Hooker and E.R. Firestone, Eds., NASA Goddard Space Flight Center, Greenbelt, Maryland, 60 pp.

——, 1995: "Comparison of Irradiance Immersion Coefficients for Several Marine Environmental Radiometers (MERs)." In: Mueller, J.L., R.S. Fraser, S.F. Biggar, K.J. Thome, P.N. Slater, A.W. Holmes, R.A. Barnes, C.T. Weir, D.A. Siegel, D.W. Menzies, A.F. Michaels, and G. Podesta: Case Studies for SeaWiFS Calibration and Validation, Part 3. *NASA Tech. Memo. 104566, Vol. 27,* S.B. Hooker, E.R. Firestone, and J.G. Acker, Eds., NASA Goddard Space Flight Center, Greenbelt, Maryland, 46 pp.

——, 2000: "Overview of Measurement and Data Analysis Protocols" In: G.S. Fargion and J.L. Mueller, Ocean Optics Protocols for Satellite Ocean Color Sensor Validation, Revision 2. *NASA Tech. Memo. 2000–209966,* NASA Goddard Space Flight Center, Greenbelt, Maryland, 87–97.

——, 2002: "Overview of Measurement and Data Analysis Protocols." In: J.L. Mueller and G.S. Fargion, Ocean Optics Protocols for Satellite Ocean Color Sensor Validation, Revision 3, Volume 1. *NASA Tech. Memo. 2002–210004/Rev3–Vol1,* NASA Goddard Space Flight Center, Greenbelt, Maryland, 123–137.

——, 2003: "Overview of Measurement and Data Analysis Methods." In: J.L. Mueller and 17 Coauthors, Ocean Optics Protocols for Satellite Ocean Color Sensor Validation, Revision 4, Volume III: Radiometric Measurements and Data Analysis Protocols. *NASA Tech. Memo. 2003–211621/Rev4–Vol.III,* NASA Goddard Space Flight Center, Greenbelt, Maryland, 1–6.

——, and R.W. Austin, 1992: Ocean Optics Protocols for SeaWiFS Validation. *NASA Tech. Memo. 104566, Vol. 5,* S.B. Hooker and E.R. Firestone, Eds., NASA Goddard Space Flight Center, Greenbelt, Maryland, 43 pp.

——, B.C. Johnson, C.L. Cromer, J.W. Cooper, J.T. McLean, S.B. Hooker, and T.L. Westphal, 1994: The Second SeaWiFS Intercalibration Round-Robin Experiment, SIRREX-2, June 1993. *NASA Tech. Memo. 104566, Vol. 16,* S.B. Hooker and E.R. Firestone, Eds., NASA Goddard Space Flight Center, Greenbelt, Maryland, 121 pp.

——, and R.W. Austin, 1995: Ocean Optics Protocols for SeaWiFS Validation, Revision 1. *NASA Tech. Memo. 104566, Vol. 25,* S.B. Hooker, E.R. Firestone, and J.G. Acker, Eds., NASA Goddard Space Flight Center, Greenbelt, Maryland, 66 pp.

——, B.C. Johnson, C.L. Cromer, S.B. Hooker, J.T. McLean, and S.F. Biggar, 1996: The Third SeaWiFS Intercalibration Round-Robin Experiment (SIRREX-3), 19–30 September 1994. *NASA Tech. Memo. 104566, Vol. 34,* S.B. Hooker, E.R. Firestone, and J.G. Acker, Eds., NASA Goddard Space Flight Center, Greenbelt, Maryland, 78 pp.

——, and A. Morel, 2003: "Fundamental Definitions, Relationships and Conventions." In: J.L. Mueller and 4 Coauthors, Ocean Optics Protocols for Satellite Ocean Color Sensor Validation, Revision 4, Volume I: Radiometric Measurements and Data Analysis Protocols. *NASA Tech. Memo. 2003–211621/Rev4–Vol.I,* NASA Goddard Space Flight Center, Greenbelt, Maryland, 11–30.

O'Reilly, J.E., S. Maritorena, B.G. Mitchell, D.A. Siegel, K.L. Carder, S.A. Garver, M. Kahru, and C. McClain, 1998: Ocean color chlorophyll algorithms for SeaWiFS. *J. Geophys. Res.,* **103,** 24,937–24,953.

——, and 24 Coauthors, 2000: SeaWiFS Postlaunch Calibration and Validation Analyses, Part 3. *NASA Tech. Memo. 2000–206892, Vol. 11,* S.B. Hooker and E.R. Firestone, Eds., NASA Goddard Space Flight Center, 49 pp. 1,907–1,925.

Riley, T., and S. Bailey, 1998: The Sixth SeaWiFS/SIMBIOS Intercalibration Round-Robin Experiment (SIRREX-6) August–December 1997. *NASA Tech. Memo. 1998–206878,* NASA Goddard Space Flight Center, Greenbelt, Maryland, 26 pp.

Siegel, D.A., M.C. O'Brien, J.C. Sorensen, D. Konnoff, E.A. Brody, J.L. Mueller, C.O. Davis, W.J. Rhea, and S.B. Hooker, 1995: Results of the SeaWiFS Data Analysis Round-Robin (DARR), July 1994. *NASA Tech. Memo. 104566, Vol. 26,* S.B. Hooker and E.R. Firestone, Eds., NASA Goddard Space Flight Center, Greenbelt, Maryland, 58 pp.

Smith, R.C., and K.S. Baker, 1984: The analysis of ocean optical data. *Ocean Optics VII,* M. Blizard, Ed., *SPIE,* **478,** 119–126.

Toole, D.A., D.A. Siegel, D.W. Menzies, M.J. Neumann, and R.C. Smith, 2000: Remote sensing reflectance determinations in the coastal ocean environment—impact of instrumental characteristics and environmental variability. *Appl. Opt.,* **39,** 456–469.

Zibordi, G., J.P. Doyle, and S.B. Hooker, 1999: Offshore tower shading effects on in-water optical measurements. *J. Atmos. Oceanic Tech.,* **16,** 1,767–1,779.

——, D. D'Alimonte, D. van der Linde, J-F. Berthon, S.B. Hooker, J.L. Mueller, G. Lazin, and S. McLean, 2002: The Eighth SeaWiFS Intercalibration Round-Robin Experiment (SIRREX-8), September–December 2001. *NASA Tech. Memo. 2002–206892, Vol. 20,* S.B. Hooker and E.R. Firestone, Eds., NASA Goddard Space Flight Center, Greenbelt, Maryland, 39 pp.

——, F. Mélin, S.B. Hooker, D. D'Alimonte, and B. Holben, 2004: An autonomous above-water system for the validation of ocean color radiance data. *Trans. IEEE Trans. Geosci. Remote Sensing.,* **42,** 401–415.

——, B. Holben, S.B. Hooker, F. Mélin, J-F. Berthon, I. Slutsker, D. Giles, D. Vandemark, H. Feng, K. Rutledge, G. Schuster, and A. Al Mandoos, 2006: A Network for Standardized Ocean Color Validation Measurements. *Eos, Trans. Amer. Geophys. Union*, **84,** 293, 297.